S & M 4169

Sustainable Rice Husk-derived Porous Carbon as an Electrode Modifier for Electrochemical Lead Detection

Yong-Gu Lee¹ and Sungnam Hong^{2*}

¹Environmental Research Institute, Kangwon National University, 1, Kangwondaehak-gil, Chuncheon-si, Gangwon-do 24341, Republic of Korea ²Department of Ocean Civil Engineering, Gyeongsang National University, 2, Tongyeonghaean-ro, Tongyeong City, Gyeongnam 53064, Republic of Korea

(Received September 1, 2025; accepted September 22, 2025)

Keywords: rice husk-derived porous carbon, electrochemical sensor, screen-printed electrode, lead detection, environmental monitoring

Heavy metal contamination poses serious threats to public health and ecosystems, with lead (Pb²⁺) being among the most hazardous owing to its persistence and toxicity. Rapid, costeffective, and portable Pb2+ detection is therefore essential for environmental monitoring. In this study, rice husk-derived porous carbon (RHPC) was synthesized at three carbonization temperatures (350, 450, and 550 °C) and applied as a modifier for screen-printed electrodes (SPEs). RHPC suspensions were drop-cast on SPE surfaces and evaluated by square-wave anodic stripping voltammetry (SWASV). Structural characterization revealed increased porosity, higher surface area, and enhanced conductivity with rising carbonization temperature, with RHPC-550 showing the most favorable properties. Electrochemical measurements confirmed that RHPC-550-SPE achieved a markedly improved electrochemically active surface area (0.030 cm²) compared with the bare SPE (0.009 cm²). As a result, RHPC-550-SPE exhibited a higher sensitivity (0.037 μ A/ μ g·L⁻¹), a lower detection limit (1.6 μ g/L vs. 6.2 μ g/L for bare SPE), and an excellent linearity ($R^2 > 0.999$) across 0–200 µg/L. Furthermore, negligible interference from common ions was observed, confirming reliable selectivity. These findings demonstrate that RHPC-modified SPEs provide a sustainable and low-cost sensing platform for trace Pb2+ monitoring in environmental applications.

1. Introduction

Heavy metal contamination has become a critical global issue, underscoring the importance of developing reliable tools for monitoring toxic elements in the environment.⁽¹⁾ Among these pollutants, lead (Pb²⁺) stands out as one of the most dangerous heavy metals owing to its widespread use, non-biodegradable nature, and severe toxicity.⁽²⁾ Lead released into the environment can persist and bioaccumulate, and even low-level exposure is associated with serious health effects, including neurological damage, kidney dysfunction, and developmental

disorders in children.⁽³⁾ The urgent need to monitor and control lead contamination has therefore gained increased attention in recent years.

Conventional analytical methods for detecting lead rely on well-established analytical techniques, including atomic absorption spectroscopy (AAS), inductively coupled plasma-based optical emission or mass spectrometry (ICP-OES/MS), high-performance liquid chromatography, and various colorimetric or fluorescence assays.⁽⁴⁾ These methods offer high sensitivity and accuracy for trace Pb²⁺ analysis; however, they suffer from significant practical limitations. In general, traditional heavy metal assays require expensive instrumentation, time-consuming sample preparation, and skilled operators, which render them impractical for rapid on-site or field applications.⁽⁵⁾ As a result, there is a growing demand for alternative lead detection approaches that are more cost-effective, portable, and capable of providing real-time results.

Electrochemical sensors have emerged as a promising alternative for detecting heavy metals, addressing many of the drawbacks of conventional techniques. In contrast to lab-bound methods, electrochemical detection systems (for example, anodic stripping voltammetry) are relatively low-cost, simple to operate, and capable of delivering rapid responses, making them well-suited for the on-site monitoring of metal contaminants.⁽⁶⁾ These sensors can achieve excellent sensitivity and selectivity for target ions by transducing chemical interactions into measurable electrical signals. Notably, the accessibility and portability of electrochemical sensors allow the frequent *in-situ* testing of water or soil for Pb²⁺, which is crucial for the early warning of pollution and timely risk management in environmental and public health contexts.

The performance of electrochemical sensors is critically dependent on the choice of the working electrode material. (7) The physicochemical attributes of the electrode surface—such as morphology, porosity, and surface chemistry—directly affect analyte recognition, electron-transfer kinetics, and detection sensitivity. (8) Conventional, unmodified electrodes, including bare carbon and metallic substrates, often exhibit inherent shortcomings, such as surface fouling, a restricted electroactive area, and sluggish charge-transfer efficiency. (9) To overcome these limitations, research has increasingly focused on engineering electrode surfaces through structural or compositional modifications. (10) Such strategies expand the electroactive interface, increase the density of available reaction sites, and enhance charge transport pathways, thereby yielding improved current responses and higher analytical sensitivity. Consequently, the rational design and modification of electrode materials represent a cornerstone in advancing reliable and high-performance electrochemical sensors.

Biomass-derived carbon materials have gained considerable attention as sustainable electrode modifiers owing to their high surface area, chemical stability, and tunable porosity. (11) Carbonaceous products obtained from the pyrolysis of agricultural residues, such as biochar, represent a promising class of functional materials. Rice husk (RH), an abundantly available byproduct of rice production, is particularly attractive as a renewable carbon source because it is rich in cellulose and lignin, which can be transformed into high-performance porous carbon through thermal or chemical activation. (12,13) This valorization of RH not only addresses waste management but also aligns with the principles of green chemistry, producing materials with desirable physicochemical properties, such as large surface area, hierarchical porosity, and improved conductivity. (8) Recent studies (2020–2025) have demonstrated significant progress in

electrochemical Pb2+ detection using biomass-derived carbons. Notable advances include nitrogen-doped porous structures achieving nanomolar-level sensitivity, (10) Bi/Bi₂O₃-doped metal organic framework-derived carbons showing excellent trace-level performance, (14) and the growing emphasis on combining sustainable carbon resources with rational nanostructuring as a key strategy for next-generation heavy-metal sensing technologies. (15) Nevertheless, the application of RH-derived porous carbon (RHPC) remains underexplored, particularly with respect to the systematic evaluation of carbonization conditions. Previous studies have often relied on a single pyrolysis temperature or limited thermal ranges, which restricts a comprehensive understanding of how heating profiles affect pore formation, surface chemistry, and electrical conductivity. (16,17) To overcome this limitation, in the present study, we investigate RHPC synthesized within the 350-550 °C range, which corresponds to the primary decomposition zone of rice husk. This interval provides a balance between improved porosity and electrical conductivity while retaining electroactive surface groups required for sensing. (18) Higher carbonization temperatures (≥700 °C) were excluded because they frequently lead to pore collapse, the depletion of functional groups, and excessive energy demands without proportionate benefits in sensing performance. (19) On this basis, the objective of this work is to fabricate a low-cost and environmentally friendly electrochemical sensor for Pb2+ by employing RHPC as an electrode modifier. With its hierarchical porosity and functional surface sites, RHPC is expected to facilitate electron transport and analyte adsorption, thereby achieving a sensitive, selective, and field-deployable monitoring of lead pollution in environmental waters.

2. Materials and Methods

2.1 Chemicals and reagents

RH was acquired from a rice mill in Suncheon-si, Jeollanam-do, Republic of Korea. The material was rinsed several times with deionized (DI) water (Human, Seoul, Republic of Korea) to eliminate surface dust and residual impurities, followed by drying at 105 °C for 24 h. Sulfuric acid (H₂SO₄, 95–98%), nitric acid (HNO₃, 70%), potassium chloride (KCl, ≥99.0%), potassium ferricyanide (K₃[Fe(CN)₆], 99%), and lead(II) nitrate [Pb(NO₃)₂, 99.999%] were purchased from Sigma-Aldrich (St. Louis, MO, USA). All aqueous solutions were prepared with DI water having a resistivity greater than 18.2 MΩ·cm.

2.2 Preparation of RHPC

The precleaned RH was subjected to pyrolysis in a rotary kiln furnace (Purnnature, Suncheon-si, Republic of Korea) under oxygen-limited conditions. Carbonization was performed at three target temperatures (350, 450, and 550 °C) using a heating rate of 10 °C/min and a holding time of 1 h. The resulting samples were denoted as RHPC-350, RHPC-450, and RHPC-550, respectively. After naturally cooling under an inert atmosphere, the carbonized materials were pulverized and sieved through a 75-mesh screen prior to subsequent experiments.

2.3 Characterization of RHPC samples

The morphological features and elemental composition of RHPCs were analyzed by scanning electron microscopy (SEM, S-4800, Hitachi, Tokyo, Japan) with energy-dispersive X-ray spectroscopy (EDX). Functional groups on the surface were identified by Fourier-transform infrared (FT-IR) spectroscopy (iN10/iS50, Thermo Fisher Scientific, Madison, WI, USA) in the range of 400–4000 cm⁻¹. Nitrogen adsorption—desorption isotherms at 77 K were recorded to evaluate textural properties, including surface area, pore volume, and pore size distribution, which were calculated by the Brunauer–Emmett–Teller (BET) method (BELSORP MAX, Microtrac Bel Inc., York, USA).

2.4 Modification of screen-printed electrodes

Screen-printed electrodes (SPEs) were modified with each type of RHPC (350, 450, and 550 °C). Briefly, finely ground RHPC powders were dispersed in a 0.01 wt% Nafion solution prepared in an 80:20 (v/v) ethanol:DI water mixture at a concentration of 1 mg/mL. The suspensions were ultrasonicated for 30 min to achieve uniform dispersion. A 5 μ L aliquot of the suspension was then drop-cast onto the working electrode (WE) area of the SPE and allowed to dry at room temperature (20 \pm 0.5 °C). The modified electrodes were stored in a desiccator until the electrochemical analysis was performed.

2.5 Electrochemical measurements

Electrochemical measurements were conducted using a portable potentiostat/galvanostat (PalmSens 4, Palm Instruments BV, The Netherlands) with PSTrace software (v. 5.11). Experiments were performed at ambient temperature without stirring or oxygen removal. The SPEs (The BIO Co. Ltd., Republic of Korea) consisted of a carbon WE (geometric area: 0.028 cm²), a carbon counter electrode, and an integrated Ag/AgCl reference electrode, with a dedicated connector ensuring stable contact. Cyclic voltammetry (CV) was performed in 5 mM [Fe(CN)₆]^{3-/4-} containing 0.1 M KCl at scan rates of 10–100 mV/s to evaluate electron transfer characteristics. For Pb2+ detection, a 1,000 mg/L stock solution of Pb(NO3)2 in 1% (v/v) HNO3 was used to prepare working standards (0-200 µg/L) by serial dilution in 0.1 M KCl (pH 4.0, 0.05 M acetate buffer). Measurements were performed by square wave anodic stripping voltammetry (SWASV) under the following conditions: conditioning at -0.18 V for 30 s, deposition at -1.10 V for 300 s, equilibration for 10 s, and potential scanning from -1.10 to 0 V versus Ag/AgCl. The step amplitude, pulse amplitude, and frequency were set to 5 mV, 25 mV, and 15 Hz, respectively. Calibration curves were generated by plotting stripping peak currents against Pb²⁺ concentration (0, 2.5, 5, 10, 20, 40, 60, 80, 100, and 200 μg/L), with each level analyzed in triplicate (n = 3). Error bars represent standard deviations of replicates. Procedural blanks (supporting electrolyte without Pb²⁺) were included to confirm baseline stability, and the limit of detection (LOD) was determined as 3σ /slope, where σ is the standard deviation of blank measurements. (20) Finally, Student's t-tests ($\alpha = 0.05$) were performed at selected concentrations to confirm that the performance differences between RHPC-550-SPE and bare SPE were statistically significant (p < 0.05).⁽²¹⁾

2.6 Electrochemical active surface area (ECSA) calculation

The ECSA of the electrodes was estimated from CV experiments using the well-established Randles–Sevcik relation:⁽²²⁾

$$I_p = (2.69 \times 105) n^{3/2} D^{1/2} AC v^{1/2},$$
 (1)

where I_p is the peak current (A), n is the number of electrons presented in half-reaction for the redox couple (n=1), $D=6.2\times 10^{-6}~\rm cm^2/s$ (the diffusion coefficient of $[\rm Fe(CN)_6]^{3^{-/4-}}$), $C=5.0\times 10^{-6}~\rm mol/cm^3$ (the concentration of $[\rm Fe(CN)_6]^{3^{-/4-}}$), and v is the potential scan rate (V/s) to determine the ECSA = A (cm²). CV measurements were performed in 5 mM $[\rm Fe(CN)_6]^{3^{-/4-}}$ containing 0.1 M KCl at scan rates ranging from 20 to 100 mV/s. The anodic peak currents were plotted against the square root of the scan rate ($v^{1/2}$), and the slope of the linear regression was used to calculate the ECSA in accordance with the Randles–Sevcik relation.

3. Results and Discussion

3.1 Modification of SPEs

Figure 1 shows SEM images of the RHPCs carbonized at 350, 450, and 550 °C. A clear evolution in morphology is observed with increasing carbonization temperature. RHPC-350 exhibits a relatively dense, chunk-like structure with few visible pores, whereas RHPC-450 and RHPC-550 display progressively more porous and fragmented textures [Figs. 1(a)–1(c)]. These suggest that higher carbonization temperatures facilitate the development of porosity within the carbonized RH matrix.⁽²³⁾

Consistently, the BET surface area of the RHPCs increases from 42.8 m²/g at 350 °C to 135.7 m²/g at 550 °C, as listed in Table 1. The total pore volume more than doubles (from 0.21 to 0.52 cm³/g) and the average pore diameter grows from ~1.3 to ~1.9 nm over the same temperature range (Table 1), suggesting the formation of additional micropores and the slight widening toward mesoporous dimensions at higher carbonization temperatures. Such growth in porosity can be attributed to the more extensive decomposition and volatilization of biomass components at elevated temperatures. Notably, the average pore sizes remain in the sub-2 nm range, indicating that the RHPCs are predominantly microporous carbons even at 550 °C. This trend aligns with the known thermal analysis of RH, which indicates significant mass loss (i.e., decomposition of carbonaceous matter) occurring between ~350 and 550 °C. By ~550 °C, most organic constituents have carbonized or vaporized, leaving behind a more developed carbon pore network and an inorganic ash (primarily SiO₂) structure as a template. (24) The electrical conductivity of the RHPCs also improves markedly with increasing carbonization temperature (Table 1). RHPC-350 has a conductivity of 286.3 μS/cm, which rises to 396.9 μS/cm for RHPC-

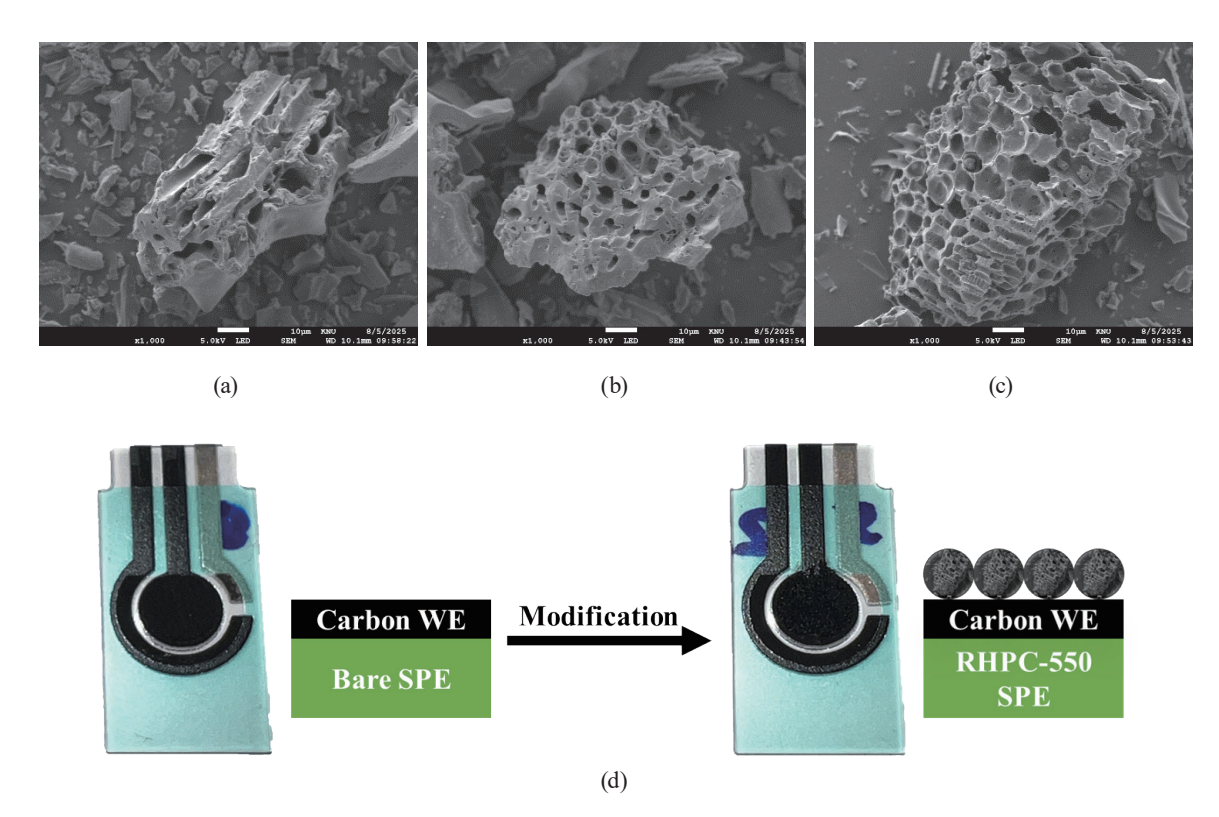


Fig. 1. (Color online) SEM images of (a) RHPC-350, (b) RHPC-450, and (c) RHPC-550. (d) Schematic diagram of the modification of RHPC-550 on bare SPE for detecting Pb²⁺.

Table 1 Physicochemical properties of RHPC-350, RHPC-450, and RHPC-550 (n = 3, mean \pm standard deviation).

	RHPC-350	RHPC-450	RHPC-550
Specific surface area (m ² /g)	42.82 ± 3.00	82.83 ± 5.80	135.66 ± 9.50
Total pore volume (cm ³ /g)	0.21 ± 0.02	0.40 ± 0.03	0.52 ± 0.04
Average pore diameter (nm)	1.26 ± 0.09	1.36 ± 0.10	1.85 ± 0.13
Electrical conductivity (µS/cm)	286.24 ± 4.00	396.86 ± 5.80	410.89 ± 6.90

450 and further to 410.9 μ S/cm for RHPC-550. This ~40% increase from 350 to 550 °C reflects the enhanced graphitization and purity of the carbon matrix at higher temperatures. Elevated carbonization temperatures drive off more of the insulating heteroatoms (O, H) and volatile residues, yielding a carbon framework with greater sp² character and connectivity, thereby facilitating electron transport. A similar positive correlation between heat-treatment temperature and conductivity has been reported for RH-derived carbons in the literature. (25)

Figure 2 presents the FT-IR spectra of RHPC-350, RHPC-450, and RHPC-550, which provide insight into their surface functional groups. The spectrum of RHPC-350 shows several notable absorption bands indicative of residual-oxygen-containing functionalities. A broad band around ~3400 cm⁻¹ (O–H stretching) and features near ~1700 cm⁻¹ (C=O stretching of carbonyl or carboxyl groups) are observed in RHPC-350, suggesting the presence of hydroxyl groups (from adsorbed water or phenolic OH) and carbonyl/carboxylic groups on the carbon surface. Peaks in the region of 1000–1150 cm⁻¹ are also evident, which could be attributed to C–O stretching

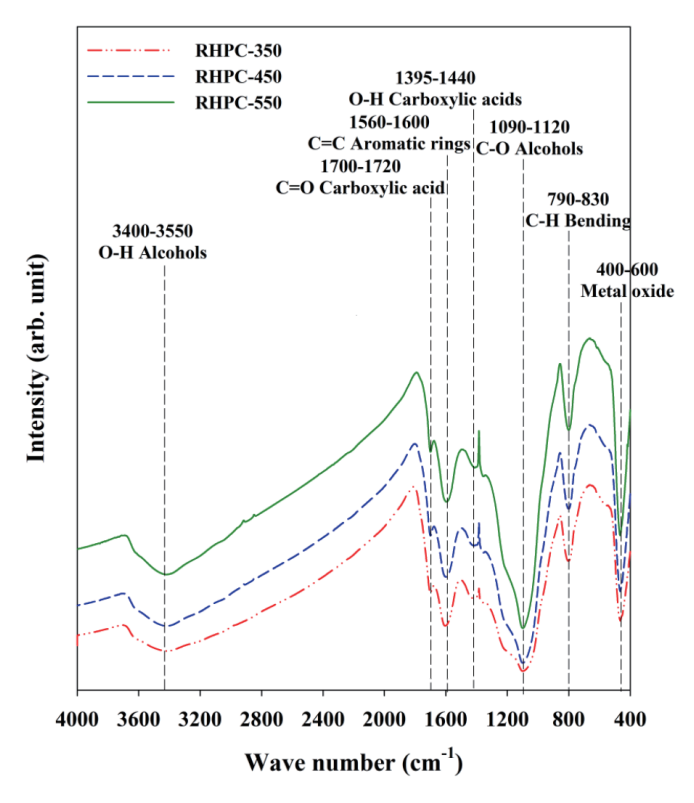


Fig. 2. (Color online) FT-IR spectra of RHPC-350, RHPC-450, and RHPC-550.

vibrations or Si–O–Si bonds from the silica content of RHPC. As the carbonization temperature increases, the signals from these polar functional groups diminish substantially. In RHPC-550, the O–H and C=O bands are greatly weakened or absent in the FT-IR spectrum (Fig. 2), indicating that most of the surface oxygen complexes have been eliminated at the highest treatment temperature. This trend of decreasing surface functionality with increasing pyrolysis temperature is expected, as a more severe thermal treatment breaks down oxygenated structures (releasing CO, CO₂, and so forth) and leaves behind a more graphitic carbon surface.⁽²⁶⁾

3.2 Estimation of electrochemical active surface area of modified RHPCs-SPEs

Table 2 shows that the bare SPE exhibited a very small ECSA of approximately 0.009 cm², only ~32% of its nominal geometric area. This finding indicates that nearly two-thirds of the printed carbon surface is electrochemically inaccessible, most likely owing to the presence of binders and the limited number of edge-plane sites available for charge transfer. Such low intrinsic electroactivity is commonly observed in printed carbon electrodes and highlights the necessity of surface modification. (27) Upon modification with RHPC, the electrodes demonstrated a clear enhancement in ECSA. At the lowest carbonization temperature (RHPC-350), the ECSA increased to 0.016 cm², almost twice that of the bare SPE. Further carbonization to 450 °C yielded an ECSA of 0.021 cm², while RHPC-550 reached 0.030 cm². Remarkably, RHPC-550-SPE surpassed the geometric area, corresponding to ~107% of the nominal surface

Electrochemical acti	ve surface area of m	odilied KHPC-SPES.	
Electrode	ECSA (cm ²)	$ECSA$ /Geometric area ($WE = 0.028 \text{ cm}^2$)	Slope (µA/V/s)
Bare SPE	0.009	0.32	_
RHPC-350-SPE	0.016	0.57	1.093×10^{-4}
RHPC-450-SPE	0.021	0.75	1.413 × 10 ⁻⁴
RHPC-550-SPF	0.030	1.07	1 988 × 10 ⁻⁴

Table 2
Electrochemical active surface area of modified RHPC-SPEs

and more than threefold the ECSA of the bare SPE. The observed increase in ECSA with pyrolysis temperature is consistent with structural changes in the RHPCs, including the improved conductivity, enhanced porosity, and greater exposure of defect sites, as confirmed by BET and SEM results (see Sect. 3.1, Fig. 1).

3.3 Enhanced detection of Pb²⁺ via RHPC-550-SPE: Performance comparison with bare SPE

To evaluate the electrochemical performance of RHPC-550-SPE for Pb2+ detection, measurements were carried out across the concentration range of 0–200 μg/L and the obtained results were compared with data for the bare SPE under identical conditions. All measurements were performed in triplicate, and the results are reported with error bars representing the standard deviation (n = 3). As shown in Fig. 3, RHPC-550-SPE consistently produced higher current responses than the bare SPE. At 2.5 μ g/L, RHPC-550-SPE produced a peak of 0.10 \pm $0.01~\mu A$, compared with $0.04 \pm 0.005~\mu A$ for the bare SPE. At the highest concentration (200 μ g/L), RHPC-550-SPE reached 7.5 \pm 0.2 μ A, while the bare SPE recorded only 4.8 \pm 0.3 μ A. This enhancement is attributed to the larger electroactive surface area and the presence of surface functionalities in the RHPC material, which promote Pb2+ adsorption and accelerate electron transfer.⁽²⁸⁾ The calibration plots further highlight the superior performance of RHPC-550-SPE, which exhibited a steeper slope (0.037 μA/μg·L⁻¹) than 0.024 μA/μg·L⁻¹ for the bare SPE. The LOD was determined to be 1.6 μg/L for RHPC-550-SPE and 6.2 μg/L for the bare SPE. Statistical validation using Student's t-tests at representative concentrations (2.5, 50, and 200 μ g/L) confirmed that these differences were significant (p < 0.05), supporting the reproducibility and robustness of the improved performance. Overall, RHPC-550-SPE provided a lower detection limit, a higher sensitivity, and a broader dynamic range than the bare SPE, making it highly suitable for trace-level Pb2+ monitoring in environmental water samples. Notably, the LOD obtained in this study for Pb²⁺ in aqueous solution (pH 4.0) is comparable to that reported for other Pb²⁺ electrochemical sensors developed under acidic conditions, (6,10) further confirming the competitiveness of RHPC-550-SPE as a sensing platform.

3.4 Effect of interfering ions on Pb2+-detecting RHPC-550-SPE

To assess the selectivity of the proposed RHPC-550-SPE for Pb²⁺, voltametric responses were recorded in 0.1 M KCl (pH 4.0) containing a fixed amount of Pb²⁺ (100 μg/L) in the absence and presence of potentially interfering ions. Each interferent, Na⁺, K⁺, Ca²⁺, Mg²⁺, Cl⁻, and SO₄²⁻,

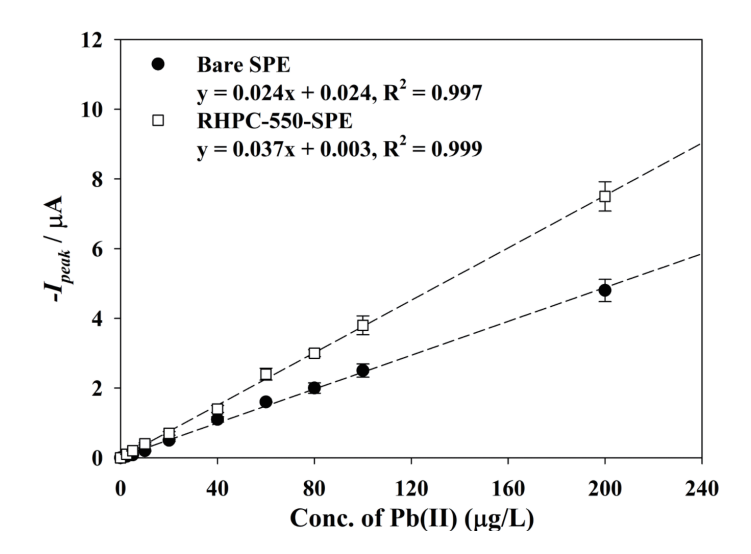


Fig. 3. Pb2+ determination using RHPC-550-SPE and bare SPE at various concentrations (0 – 200 μ g/L, pH 4.0).

Table 3 Selectivity of the Pb²⁺-detecting RHPC-550-SPE in the presence of interfering ions.

Interfering species	Na ⁺	K ⁺	Ca ²⁺	Mg ²⁺	Cl ⁻	SO ₄ ²⁻
Log kijamp	n.i.	n.i.	n.i.	n.i.	n.i.	n.i.

n.i. = no interference

representative of common constituents in natural waters,⁽²⁹⁾ was introduced at a 500-fold higher concentration than Pb²⁺. The amperometric selectivity coefficient $\log k_{i,j}^{amp}$ was computed according to⁽³⁰⁾

$$\log k_{i,j}^{amp} = \frac{(I_t - I_i)C_i}{I_i C_j}, \tag{2}$$

where i and j denote the analyte (Pb²⁺) and the interfering species, respectively; C is the concentration; Ii is the current due solely to the analyte; and I_t is the total current measured in the presence of both the analyte and the interferent. As summarized in Table 3, the resulting log $k_{i,j}^{amp}$ values indicate that RHPC-550-SPE experiences negligible interference in Pb²⁺ determination under the tested conditions.

5. Conclusions

In this study, the successful utilization of rice husk waste to develop porous carbon materials for electrochemical sensing applications is highlighted. Increasing carbonization temperature markedly improved the physicochemical properties of RHPCs, including surface area (42.8 to 135.7 m²/g) and conductivity (286 to 411 μ S/cm). These enhancements led to a substantial increase in the ECSA of RHPC-modified SPEs, with RHPC-550-SPE exhibiting an ECSA of

0.030 cm², which is more than three times higher than that of the bare SPE (0.009 cm²). The improved structural and electrical properties translated into superior Pb²+ detection performance. RHPC-550-SPE showed a higher sensitivity, a broader linear range, and a lower detection limit (1.6 µg/L), which is below the World Health Organization (WHO) guideline value of 10 µg/L for drinking water. Additionally, the electrode demonstrated excellent selectivity against major interfering ions, confirming its reliability in complex water matrices. Overall, RHPC-550-SPE provides an environmentally friendly and cost-effective sensing platform that combines waste valorization with practical environmental monitoring. The results of this work not only advance the field of biomass-derived electrode materials but also establish a pathway toward scalable, field-deployable heavy-metal detection systems.

Acknowledgments

This work was supported by the National Research Foundation of Korea (NRF) grant founded by the Korea government (MSIT) (RS-2023-00250939).

References

- 1 G. Ondrasek, J. Shepherd, S. Rathod, R. Dharavath, M. I. Rashid, M. Brtnicky, M. S. Shahid, J. Horvatinec, and Z. Rengel: RSC Adv. 15 (2025) 3904. https://doi.org/10.1039/D4RA04639K
- 2 U. Kamran, S.-Y. Lee, K. Y. Rhee, and S.-J. Park: Chemosphere 323 (2023) 138210. https://doi.org/10.1016/j.chemosphere.2023.138210
- 3 M. Zaynab, R. Al-Yahyai, A. Ameen, Y. Sharif, L. Ali, M. Fatima, K. A. Khan, and S. Li: J. King Saud Univ. Sci. **34** (2021) 101653. https://doi.org/10.1016/j.jksus.2021.101653
- 4 M. Aish, R. F. Alshehri, A. S. Amin, and H. H. El-Feky: Talanta Open **8** (2023) 100253. https://doi.org/10.1016/j.talo.2023.100253
- 5 Y. Li, H. Huang, R. Cui, D. Wang, Z. Yin, D. Wang, L. Zheng, J. Zhang, Y. Zhao, H. Yuan, J. Dong, X. Guo, and B. Sun: Sens. Actuators, B 332 (2021) 129519. https://doi.org/10.1016/j.snb.2021.129519
- 6 Y.-G. Lee, J. Han, S. Kwon, S. Kang, and A. Jang: Chemosphere **143** (2016) 78. https://doi.org/10.1016/j.chemosphere.2015.05.069
- 7 E. Bakker and M. Telting-Diaz: Anal. Chem. 74 (2002) 2781. https://doi.org/10.1021/ac0202278
- 8 P. Noppawan, J. Jakmunee, A. J. Hunt, N. Supanchaiyamat, S. Sangon, J. Lerdsri, T. Kruatian, and J. Upan: Sci. Rep. 15 (2025) 18380. https://doi.org/10.1038/s41598-025-03405-w
- 9 A. J. S. Ahammad, M. M. Hasan, T. Islam, M. O. Al-Shehri, A. N. Anju, M. K. Alam, J.-P. Kim, M. A. A. Qasem, and M. A. Aziz: New J. Chem. **42** (2018) 4543. https://doi.org/10.1039/C7NJ04777K
- 10 R. Sharma, D. S. Rana, A. Awasthi, D. Singh, A. A. Ibrahim, A. Umar, and S. Baskoutas: Heliyon **10** (2024) e39090. https://doi.org/10.1016/j.heliyon.2024.e39090
- 11 D. Spanu, G. Binda, C. Dossi, and D. Monticelli: Microchem. J. **159** (2020) 105506. https://doi.org/10.1016/j.microc.2020.105506
- 12 M. A. Haque, M. M. Hasan, T. Islam, M. A. Razzak, N. H. Alharthi, A. Sindan, M. R. Karim, S. I. Basha, M. A. Aziz, and A. J. S. Ahammad: Electroanalysis 32 (2020) 1957. https://doi.org/10.1002/elan.202060059
- 13 M. Mehmandoust, G. Li, and N. Erk: Ind. Eng. Chem. Res. **62** (2023) 4628. https://doi.org/10.1021/acs.iecr.2c03058
- 14 C. Wang, Q. Niu, D. Liu, X. Dong, and T. You: Talanta **258** (2023) 124281. https://doi.org/10.1016/j.talanta.2023.124281
- 15 C. Onfray and A. Thiam: Micromachines 14 (2023) 1688. https://doi.org/10.3390/mi14091688
- 16 I. Lobzenko, M. Burachevskaya, I. Zamulina, A. Barakhov, T. Bauer, S. Mandzhieva, S. Sushkova, T. Minkina, A. Tereschenko, V. Kalinichenko, O. Khroniuk, and V. D. Rajput: Agriculture 12 (2022) 1689. https://doi.org/10.3390/agriculture12101689
- 17 X. Wang, Z. Lu, L. Jia, and J. Chen: Results Phys. 6 (2016) 866. https://doi.org/10.1016/j.rinp.2016.09.011
- 18 H. Lyu, Z. Yu, B. Gao, F. He, J. Huang, J. Tang, and B. Shen: Environ. Sci. Pollut. Res. 26 (2019) 14693. https://doi.org/10.1007/s11356-019-04899-4

- 19 W. Liao, X. Zhang, S. Ke, J. Shao, H. Yang, S. Zhang, and H. Chen: Ind. Crops Prod. 186 (2022) 115238. https://doi.org/10.1016/j.indcrop.2022.115238
- 20 J. Uhrovčík: Talanta 119 (2014) 178. https://doi.org/10.1016/j.talanta.2013.10.061
- V. Bezerra dos Santos, E. L. Fava, N. Sá de Miranda Curi, R. C. Faria, T. B. Guerreiro, and O. Fatibello-Filho: Anal. Methods 7 (2015) 3105. https://doi.org/10.1039/C5AY00012B
- 22 M. N. Karim, J. E. Lee, and H. J. Lee: Biosens. Bioelectron. 61 (2014) 147. https://doi.org/10.1016/j.bios.2014.05.011
- 23 N. Liu, K. Huo, M. T. McDowell, J. Zhao, and Y. Cui: Sci. Rep. 3 (2013) 1919. https://doi.org/10.1038/srep01919
- 24 W. Wang, J. C. Martin, N. Zhang, C. Ma, A. Han, and L. Sun: J. Nanopart. Res. 13 (2011) 6981. https://doi.org/10.1007/s11051-011-0609-3
- 25 J. Zhang, Z. Zhong, J. Zhao, M. Yang, W. Li, and H. Zhang: Can. J. Chem. Eng. 90 (2012) 762. https://doi.org/10.1002/cjce.20549
- 26 K. Kuratani, K. Okuno, T. Iwaki, M. Kato, N. Takeichi, T. Miyuki, T. Awazu, M. Majima, and T. Sakai: J. Power Sources 196 (2011) 10788. https://doi.org/10.1016/j.jpowsour.2011.09.001
- 27 S. J. Rowley-Neale, D. A. C. Brownson, and C. E. Banks: Nanoscale **8** (2016) 15241. https://doi.org/10.1039/C6NR04220A
- 28 X. Zeng, W. Jiang, G. I. N. Waterhouse, X. Jiang, Z. Zhang, and L. Yu: Microchim. Acta 188 (2021) 393. https://doi.org/10.1007/s00604-021-05046-y
- 29 Y.-G. Lee, H. J. Lee, and A. Jang: Sens. Actuators, B **244** (2017) 157. https://doi.org/10.1016/j.snb.2016.12.114
- 30 J. Wang: Talanta 41 (1994) 857. https://doi.org/10.1016/0039-9140(94)E0079-7